nature COMMUNICATIONS

ARTICLE

https://doi.org/10.1038/s41467-020-15682-2 OPEN

Broadband frequency translation through time refraction in an epsilon-near-zero material

Yiyu Zhou [1,4✉], M. Zahirul Alam[2,4], Mohammad Karimi[2], Jeremy Upham[2], Orad Reshef [2], Cong Liu [3], Alan E. Willner[3] & Robert W. Boyd [1,2]

Space-time duality in paraxial optical wave propagation implies the existence of intriguing effects when light interacts with a material exhibiting two refractive indexes separated by a boundary in time. The direct consequence of such time-refraction effect is a change in the frequency of light while leaving the wavevector unchanged. Here, we experimentally show that the effect of time refraction is significantly enhanced in an epsilon-near-zero (ENZ) medium as a consequence of the optically induced unity-order refractive index change in a sub-picosecond time scale. Specifically, we demonstrate broadband and controllable shift (up to 14.9 THz) in the frequency of a light beam using a time-varying subwavelength-thick indium tin oxide (ITO) film in its ENZ spectral range. Our findings hint at the possibility of designing (3 + 1)D metamaterials by incorporating time-varying bulk ENZ materials, and they present a unique playground to investigate various novel effects in the time domain.

[1] The Institute of Optics, University of Rochester, Rochester, NY 14627, USA. [2] Department of Physics, University of Ottawa, Ottawa, ON K1N 6N5, Canada. [3] Department of Electrical Engineering, University of Southern California, Los Angeles, CA 90089, USA. [4] These authors contributed equally: Yiyu Zhou, M. Zahirul Alam. ✉email: yzhou62@ur.rochester.edu

Maxwell's equations describe how an electromagnetic wave is modified by a material. The spatial boundary condition associated with Maxwell's equations can be used to derive the well-known Fresnel equations and Snell's law. A spatial variation in refractive index leads to reflection and refraction of a light beam incident on the boundary. As a consequence, the wavevector of the transmitted light changes, whereas the frequency is conserved. The spatial boundary can be abrupt (nonadiabatic) in refractive index variation such as at a glass-air interface. Or, the boundary can be smoothly varying, i.e., adiabatic in space, such as in a gradient-index lens. In both cases, the refracted beam of light must have a different k-vector (Fig. 1a), where $|k| = 2\pi n/\lambda$, n is the refractive index of the medium, and λ is vacuum wavelength of light. As the equations describing the paraxial wave propagation are unchanged upon the interchange of time and a spatial coordinate, one can define a boundary of refractive index in the time coordinate in a dual fashion to that in the spatial coordinates[1–5]. This effect is known as time refraction.

The concept of time refraction is presented in Fig. 1a. Let us assume that an optical pulse of frequency f_1 is traveling in a dispersionless medium with a refractive index of n_1. At $t = t_1$ the refractive index changes from n_1 to n_2. As a consequence of the broken time translation symmetry, the frequency of light has to change because of the change in the refractive index while leaving the wavevector unchanged[6]. The change in frequency, according to the dispersion relation $c/f = n\lambda$[7], can be expressed as $n_1 f_1 = n_2 f_2 = (n_1 + \Delta n)(f_1 + \Delta f)$, where $\Delta f = f_2 - f_1$ is the change in the frequency of light after it encounters the temporal boundary; $\Delta n = n_2 - n_1$ is the change in the refractive index; and c is the speed of light in vacuum. Consequently, we can express the change in frequency as $\Delta f = -\Delta n \cdot f_1/(n_1 + \Delta n)$. Thus, the frequency shift may be red (blue) if the change in index Δn is positive (negative). This effect is strongest when $\Delta n/(n_1 + \Delta n)$ is large. In a regular dielectric medium such as silicon[8], $\Delta n/(n_1 + \Delta n)$ can only be on the order of 10^{-3}. In contrast, in a highly nonlinear low-index medium, $\Delta n/(n_1 + \Delta n)$ can approach unity due to the near-zero linear refractive index n_1 and the large nonlinear index change Δn[9–11]. Thus, a highly nonlinear low-index medium is a natural platform with which to generate a large frequency translation using time refraction. In addition to frequency conversion, a time-varying medium with a large index change can also be used to investigate many novel effects in the time domain such as all-optical nonreciprocity[12,13], negative refraction[14], photonic topological insulators[15], photonic time crystals[16], achromatic optical switches[17], and the dynamic Casimir effect[18].

A number of effects have been used to experimentally implement a time-varying medium, such as free-carrier dispersion[19–24], Kerr nonlinearity[25–28], laser-induced plasma[29–32], and optomechanical interaction[33]. The magnitude of frequency conversion in a time-varying medium fundamentally depends on the available index change. This is in contrast to other nonlinear optical effects such as four-wave mixing[8], where the constraints of weak nonlinearity can be almost entirely overcome through use of a very long interaction length[34]. Resonant structures such as microring resonators and slow-light photonic crystals, tend to exhibit enhanced sensitivity to the change in the material's refractive index. Such resonant structures can be used to somewhat sidestep the restrictions imposed by the intrinsically low nonlinearity of materials to obtain appreciable adiabatic frequency conversion (AFC)[19–22,35–39]. Using these techniques, adiabatic frequency conversions up to 280 GHz (or ~0.145% of the carrier frequency) have been previously demonstrated[20]. Nevertheless, all prior demonstrations of AFC have exhibited the following limitations: narrow operational bandwidth[20,34,38,39]; relatively long interaction length[19,21–25,33,36,37,40]; limited tunability with respect to the magnitude and sign of shift[19–24,40]; the requirement of inhomogeneous structure limiting wide adoptions into various platforms[19–24,33,35–39]; and the possible requirement of out-of-plane above-bandgap excitation pulses[20].

Here, we show that we can simultaneously overcome all of the above-mentioned shortcomings by using a homogeneous and isotropic epsilon-near-zero (ENZ) medium of subwavelength thickness. Using a series of pump-probe measurements, we demonstrate optically controlled total frequency translations of a near-infrared beam of up to 14.9 THz (redshift of 11.1 THz and blueshift of 3.8 THz)—that is, over 6% of the bandwidth of the carrier frequency—using a 620-nm-thick ITO film. The effect of frequency translation is broadband in nature, i.e., the central wavelength of the degenerate input pump and probe pulses can be tuned over a 500 nm range. We also find that the effect is maximum near the zero-permittivity wavelength of ITO.

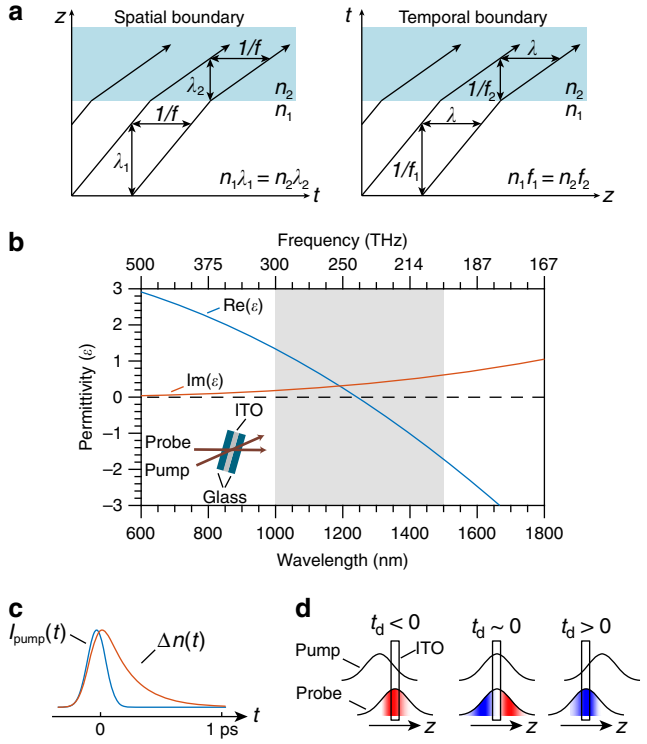

Fig. 1 Concept of time refraction. a A spatial boundary defined by a refractive index change from n_1 to n_2 leads to a change in the wavevector of a light beam as it passes through the boundary and is described by $n_1\lambda_1 = n_2\lambda_2$ (left panel). A refractive index boundary defined in time leads to time-refraction effect of a light beam as it passes through the boundary and is described by $n_1 f_1 = n_2 f_2$ (right panel). Here f is the frequency of light waves in the medium. **b** The permittivity of an ITO film used in the experiment. The inset shows the simplified experimental setup and the shaded region shows the spectral range of interest in this work. **c** Simplified illustration of the temporal index change $\Delta n(t)$ of ITO excited by a pump pulse. **d** The frequency of the probe redshifts (blueshifts) if the pump beam lags (leads) the probe. At near-zero delay both redshift and blueshift can occur.

Results

Nonlinear optical response of the ENZ material. An ENZ material is defined as a medium that has a near-zero linear permittivity, and consequently low linear refractive index. The near-zero permittivity in such a medium leads to highly non-intuitive linear effects[41–43] and strong nonlinear light-matter interactions[9,44–47]. In order to implement a temporal boundary

with a large index change, we make use of the large and ultrafast optically induced change in refractive index of a 620 nm thick ITO film in its near-zero-permittivity spectral range. ITO is a degenerately doped semiconductor and near its zero-permittivity wavelength (1240 nm), the linear permittivity of the ITO sample can be well described by the Drude model (Fig. 1b). The temporal nonlinear optical response of ITO can be described by the two-temperature model when excited by an optical pulse with a central wavelength close to the ENZ region[9,44]. The optical excitation of ITO near the ENZ region leads to a strong modification of the Fermi-Dirac distribution of the conduction band electrons. The highly nonequilibrium distribution of electrons, within the formalism of the Drude model, leads to an effective redshift of the plasma frequency owing to the momentum-dependent effective mass of the electrons. According to the two-temperature model, the rise time of the change in the refractive index is limited by the thermalization time of the conduction band electrons owing to electron-electron scattering. The rise time also depends on the energy deposition rate in the ITO film and thus has a strong dependence on the temporal envelope of the pump pulse. Once the pump pulse peak leaves the ITO film, the index returns to the initial value within a sub-picosecond time scale through electron–phonon coupling (Fig. 1c). Owing to the time-dependent nature of the index change induced by the intensity of the pump pulse, the frequency of probe pulse can be redshifted or blueshifted depending on the pump-probe delay time (see Fig. 1d).

Measurements at the near-zero-permittivity wavelength. In order to measure the magnitude of the frequency translation using ITO, we performed a set of degenerate pump-probe experiments with ~120 fs pulses and recorded the spectra of the probe beam as a function of the delay between the pump and the probe for varying pump intensities. The ITO film has two 1.1-mm-thick glass slabs on both sides. Both pump and probe beams are *p*-polarized, and the intensity of the probe beam is kept low to avoid nonlinear effects (See Methods and Supplementary Note 1 for more details). The results for $\lambda_0 = \lambda_{pump} = \lambda_{probe} = 1235$ nm at the pump-probe delay time of ±60 fs is shown in Fig. 2. The pump induces a nonlinear change in the refractive index of ITO with a rate that depends on the pump intensity, the temporal envelope of the pump, and the intrinsic nonlinear dynamics of the ITO. When the pump pulse is delayed with respect to the probe, i.e., pump-probe delay time $t_d < 0$, the probe experiences a rising refractive index and thus its spectrum redshifts (Fig. 2a). If the probe reaches the ITO after the peak of the pump pulse is passed ($t_d > 0$), it experiences a falling refractive index change and the spectrum of the probe blueshifts (Fig. 2b). We also note that for $t_d \approx 0$ both blueshift and redshift can occur (Fig. 1d). As the thickness of the ITO film is only 620 nm, 120 fs pump, and the probe pulses never reside entirely within the ITO thin film (Fig. 1d). Thus, the magnitude of the frequency shift of the probe pulse becomes dependent on the index change rate $\Delta n/\Delta t$ it experiences while transiting through the ITO film. We extract the effective values of the index change rate based on the experimental data through numerical simulations (see Supplementary Note 2). In numerical simulation we use the slowly varying envelope approximation and, as a result, the predictions of our model are only dependent on the envelope-averaged dynamics of the ITO.

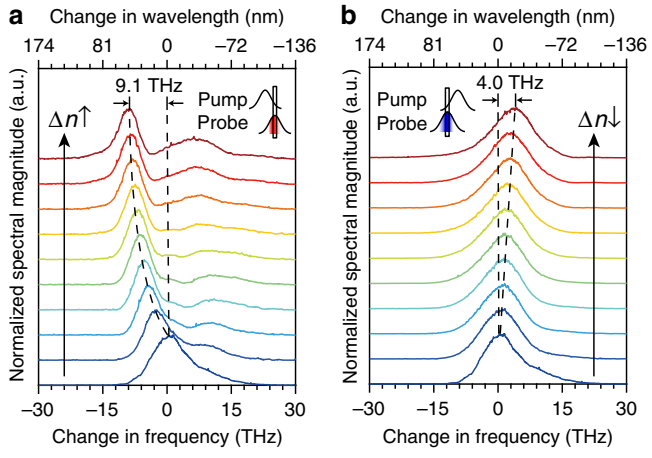

Fig. 2 Pump-induced frequency translation at a fixed delay time. a–b The frequency of a 1235 nm probe beam redshifts at the delay time $t_d = -60$ fs in **a** and blueshifts at the delay time $t_d = 60$ fs in **b**. The insets show the relative position of the pump and the probe. The top-most (bottom-most) spectra in both panels correspond to the largest (zero) pump intensity and, consequently, the largest (zero) change in the refractive index.

We find that both the pump intensity and the value of the pump-probe delay time modify the spectra of the transmitted probe. We present the results for $\lambda_0 = 1235$ nm for three pump intensities in Fig. 3a–c. In general, the time refraction leads to the modification of amplitude, bandwidth, temporal width, and the carrier frequency of the probe pulse (see Supplementary Note 3). In order to focus on the spectral shift, the magnitude of spectrum for each pump-probe delay value is individually normalized in Fig. 3. We find that when the absolute value of the pump-probe delay time $|t_d|$ is increased, the magnitude of the frequency translation for the probe decreases. Furthermore, when pump-probe delays are small, the leading portion of the probe pulse experiences an increase in refractive index (thus redshifts), whereas the trailing portion experiences a decrease of refractive index (thus blueshifts). This is evident in Fig. 3a–c by the presence of two peaks at $t_d \approx 0$. For a fixed pump-probe delay time an increase in pump intensity leads to larger change in index and, as a result, a larger shift in the central frequency of the probe pulse. Furthermore, we find that the fall time of the index change is slower than the rise time of the index change. The fall time of the index change is longer because it—within the formalism of the two-temperature model—is dictated by the intrinsic electron–phonon coupling rate, the maximum temperature of the conduction band electrons, and the thermodynamical properties of the lattice. As a result, the rate of decrease in index after the pump leaves the ITO film is smaller compared with that of the rising edge, and therefore the magnitude of the achievable redshift for a constant pump intensity is larger than the achievable blueshift. At a sufficiently high pump intensity, we observe an appearance of a large blueshifted spectral peak when the pump is at 1235 nm owing to higher-order nonlinear optical effects. At a peak pump intensity of 483 GW cm^{-2} the blueshift can be as large as 10.6 THz (~52 nm in wavelength), and the total maximum frequency translation can be larger than 20 THz (see Supplementary Note 4). This value corresponds to a fractional frequency shift ($\Delta f/f_0$) of ~9%.

We model the time-refraction effect in ITO using the nonlinear Schrödinger equation, and the split-step Fourier method is used to numerically solve the Schrödinger equation[48]. We use an iterative algorithm to calculate the approximate shape of the time-varying nonlinear phase variations induced by the index change to fit the experimentally measured spectra (see Supplementary Note 2). The simulation results are shown in Fig. 3d–f. Our numerical model is in excellent agreement with the experimental data, confirming that the origin of the shift is owing to the rapid change of index experienced by the probe pulse while transiting through the ITO sample.

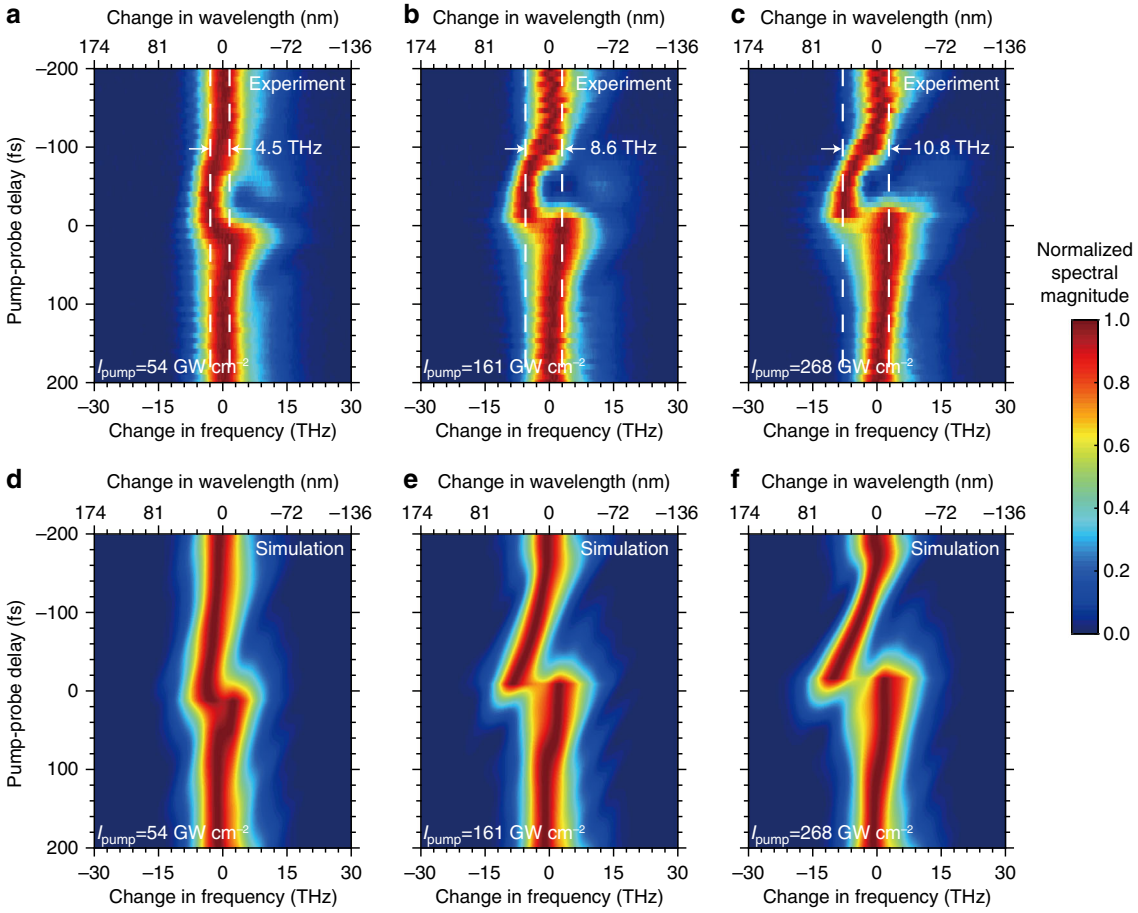

Fig. 3 Experimental and simulated probe spectra at $\lambda_0 = 1235$ nm. a–c Experimental probe spectra as a function of the pump-probe delay time for varying pump intensities. The spectral magnitude for each pump-probe delay is normalized individually. **d–f** The corresponding numerically simulated probe spectra modeled by the nonlinear Schrödinger equation. The spectra of the probe show a strong dependence on the pump intensity and pump-probe delay time. For a pump intensity of 268 GW cm^{-2}, the total frequency translation at this wavelength is 10.8 THz.

Measurements over a broad spectral range. Next, we investigate the dynamics away from the zero-permittivity wavelengths. We repeat the measurements at different excitation wavelengths from $\lambda_0 = 1000$ nm−1500 nm. For each excitation wavelength and pump intensity, we extract the maximum frequency translation of the probe over a range of pump-probe delay time (see Supplementary Note 5). We summarize the wavelength- and intensity-dependent maximum frequency translations in Fig. 4a–e. Here, we limit the pump intensities to avoid the occurrence of significant higher-order nonlinearities. Our results reveal a number of trends. First, both the total achievable frequency translation (redshift and blueshift) and the maximum achievable redshift for a constant pump intensity are the highest near 1235 nm (where $\mathrm{Re}(\varepsilon) \approx 0$) than at other wavelengths. For example, at $\lambda_0 = 1495$ nm the measured maximum magnitude of the redshift (5.4 THz) is a factor of two smaller than what can be achieved at $\lambda_0 = 1235$ nm using a lower pump intensity. Nevertheless, we find that the total maximum fractional frequency translation ($\Delta f/f_0$) at near-zero permittivity is unprecedentedly large (Fig. 4f). The maximum total frequency translation of 14.9 THz (redshift of 11.1 THz and blueshift of 3.8 THz) at $\lambda_0 = 1235$ nm (redshift plus blueshift) is over 53 times larger than what was achieved using a silicon ring resonator of a 6 μm diameter exhibiting a Q-factor greater than 18,000[20]. In contrast, the propagation distance in our material is only 620 nm which is 30 times shorter in physical length and four orders of magnitude smaller than the effective interaction length in a high-Q cavity. Moreover, our results show the operation bandwidth of ITO is much larger than what can be achieved using high-Q resonant structures.

Discussion

As the refractive index of the ENZ material depends on the intensity of the pump, the work presented here may be formally described by cross-phase modulation with a delayed response[8]. However, the concept of time refraction is independent of the source type of the index change (e.g., thermally, optomechanically, or electrically induced index change) and is a more general effect than the simple cross-phase modulation that arises when the temporal boundary is specifically induced by an optical pulse. Furthermore, in contrast to a typical four-wave-mixing-based frequency conversion, the frequency shift obtained through time refraction does not depend on the frequency difference between the pump and the probe and is completely free from phase-mismatching. Although in this work the pump and the probe are frequency degenerate and produced from the same source using a beam splitter, it is not necessary for the beams to be frequency degenerate. Nevertheless, the maximum frequency shift with minimum energy expenditure can be achieved when both the pump and the probe lie within the ENZ spectral range. As the maximum index change happens at the zero-permittivity wavelength, the probe will undergo maximum frequency shift if its wavelength is at or near the zero-permittivity wavelength, whereas the energy expenditure will be

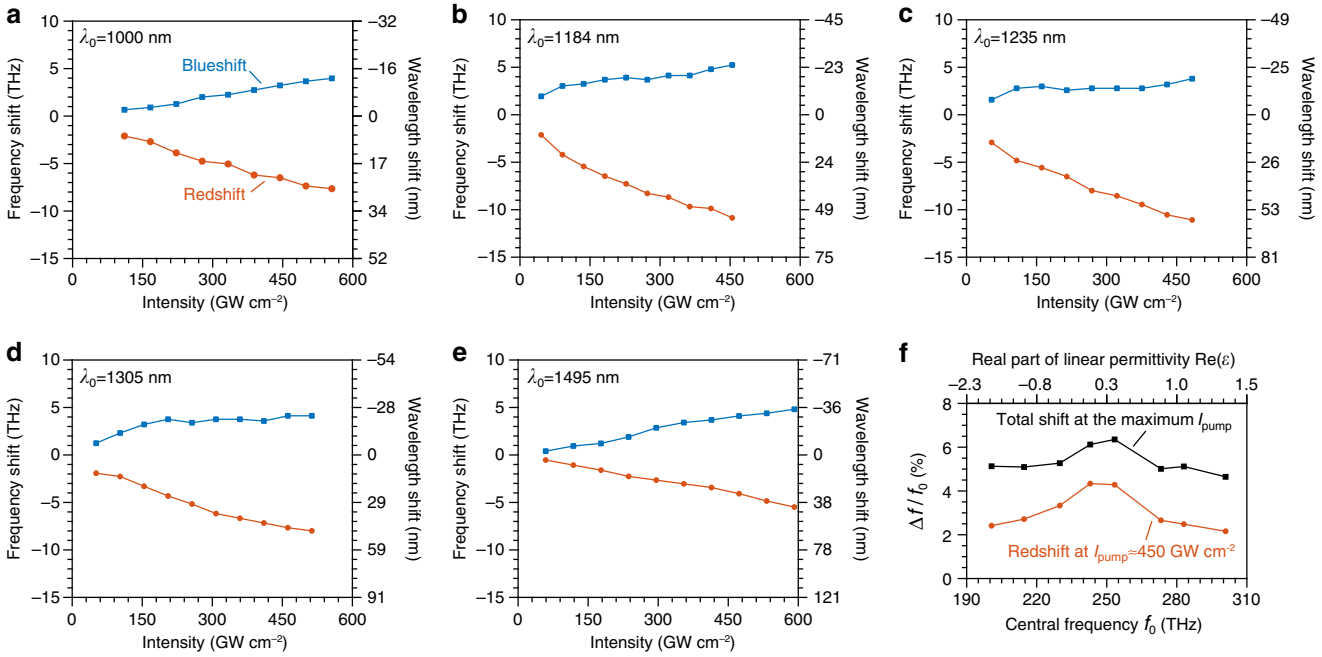

Fig. 4 Wavelength-dependent time-refraction effect. a–e Experimentally measured maximum redshifts and blueshifts at different wavelengths λ_0 as a function of peak pump intensities. **f** The red line denotes the fractional redshift $|\Delta f_{red}|/f_0$ as a function of probe beam's central frequency f_0 at a peak pump intensity ~450 GW cm^{-2}. The real part of the linear permittivity Re(ε) of ITO film at the corresponding central frequency f_0 is shown in the top axis. The black line shows the total fractional shift (redshift plus blueshift) measured at the maximum pump intensities before the onset of higher-order nonlinear optical effects. We find that both the maximum fractional redshift and the total shift occur near the zero-permittivity wavelength.

minimum if the wavelength of pump is also at or near the zero-permittivity wavelength.

In conclusion, we have shown that a subwavelength-thick ITO film can be used to obtain unprecedentedly large (~6.5% of the carrier frequency), broadband and tunable frequency translation. The large time-refraction effect in the ENZ material raises the intriguing possibility of wavelength conversion over an octave using a time-varying ENZ medium. The magnitude of the frequency translation is primarily limited by the linear loss, higher-order nonlinear optical effects, dispersion, and the interplay between the pulse width and the interaction time. We note that the ENZ spectral region of ITO and other conducting oxides can be tuned at any wavelength between 1 μm and 3 μm by choosing the appropriate doping level[49,50]. Furthermore, because the effect is present in a bulk, homogeneous and isotropic material, one can engineer nanostructures incorporating ENZ media such as plasmonic waveguides, photonic crystal waveguides, and dynamic metasurfaces to arbitrarily control the sign and the magnitude of the frequency shift in order to build efficient octave-spanning frequency tuners while simultaneously lowering the required pump power by a few orders of magnitude[9]. For example, an appropriately engineered ITO-based platform can be used to shift an entire band of optical signals in the frequency domain. Such devices may find practical usage in quantum communication protocols requiring conversion of visible photons to infrared[51] and in classical coherent optical communications[52,53]. We anticipate that the large time-refraction effect, we report here, can be exploited to engineer magnet-free nonreciprocal devices[54,55], spatiotemporal metasurfaces[13], and to investigate photonic time crystals and other topological effects in the time domain[16,56] using free-space or on-chip ENZ-based structures.

Methods

Measurements. We use a tunable optical parametric amplifier (OPA) pumped by an amplified Ti:sapphire laser of ~120 fs for the experiments. The output of the OPA is split into two beams to produce the degenerate pump and probe beams using a pellicle beam splitter. Both beams are rendered *p*-polarized. The pump beam is focused onto the sample by a 25 cm lens yielding to a spot size of ~100 μm. The probe beam is focused by a 10 cm lens and its spot diameter is ~45 μm at 1235 nm. Although the spot size can change when the wavelength of the OPA output is adjusted, we always keep the probe beam spot size significantly smaller than the pump beam so that the probe beam experiences a nearly uniform change in the refractive index in the transverse dimensions. The angles of incidences are 15° and 10° for the pump and probe, respectively. The transmitted probe light is coupled to an optical spectrum analyzer via a multimode fiber with a 50 μm core diameter. The commercially available ITO thin film (PGO GmbH) has a thickness of 310 nm and is deposited on a 1.1-mm-thick glass substrate. We sandwich two such ITO films to make the 620 nm thick ITO sample by using a customized sample holder with adjustable tightening screws (See Supplementary Note 6). We use a translation stage to control the delay time between the pump and the probe beams. The experimental setup is presented in Supplementary Note 1.

Data availability

All data supporting this study are available from the corresponding author upon request.

Code availability

All relevant computer codes supporting this study are available from the corresponding author upon request.

Received: 6 March 2020; Accepted: 19 March 2020;
Published online: 01 May 2020

References

1. Akhmanov, S., Sukhorukov, A. & Chirkin, A. Nonstationary phenomena and space-time analogy in nonlinear optics. *Sov. Phys. JETP* **28**, 748–757 (1969).
2. Kolner, B. H. Space-time duality and the theory of temporal imaging. *IEEE J. Quant. Electron* **30**, 1951–1963 (1994).
3. Xiao, Y., Maywar, D. N. & Agrawal, G. P. Reflection and transmission of electromagnetic waves at a temporal boundary. *Opt. Lett.* **39**, 574–577 (2014).
4. Xiao, Y., Agrawal, G. P. & Maywar, D. N. Spectral and temporal changes of optical pulses propagating through time-varying linear media. *Opt. Lett.* **36**, 505–507 (2011).

5. Plansinis, B. W., Donaldson, W. R. & Agrawal, G. P. What is the temporal analog of reflection and refraction of optical beams? *Phys. Rev. Lett.* **115**, 183901 (2015).
6. Mendonça, J., Guerreiro, A. & Martins, A. M. Quantum theory of time refraction. *Phys. Rev. A* **62**, 033805 (2000).
7. Mendonça, J. & Guerreiro, A. Time refraction and the quantum properties of vacuum. *Phys. Rev. A* **72**, 063805 (2005).
8. Boyd, R. W. *Nonlinear optics*. 3rd edn (Elsevier, 2003).
9. Alam, M. Z., Schulz, S. A., Upham, J., De Leon, I. & Boyd, R. W. Large optical nonlinearity of nanoantennas coupled to an epsilon-near-zero material. *Nat. Photonics* **12**, 79–83 (2018).
10. Caspani, L. et al. Enhanced nonlinear refractive index in ε-near-zero materials. *Phys. Rev. Lett.* **116**, 233901 (2016).
11. Reshef, O., De Leon, I., Alam, M. Z. & Boyd, R. W. Nonlinear optical effects in epsilon-near-zero media. *Nat. Rev. Mat.* **4**, 535–551 (2019).
12. Yu, Z. & Fan, S. Complete optical isolation created by indirect interband photonic transitions. *Nat. Photonics* **3**, 91–94 (2009).
13. Shaltout, A. M., Shalaev, V. M. & Brongersma, M. L. Spatiotemporal light control with active metasurfaces. *Science* **364**, eaat3100 (2019).
14. Pendry, J. Time reversal and negative refraction. *Science* **322**, 71–73 (2008).
15. Fang, K., Yu, Z. & Fan, S. Realizing effective magnetic field for photons by controlling the phase of dynamic modulation. *Nat. Photonics* **6**, 782–787 (2012).
16. Lustig, E., Sharabi, Y. & Segev, M. Topological aspects of photonic time crystals. *Optica* **5**, 1390–1395 (2018).
17. Williamson, I. A. & Fan, S. Broadband optical switch based on an achromatic photonic gauge potential in dynamically modulated waveguides. *Phys. Rev. Appl.* **11**, 054035 (2019).
18. Wilson, C. M. et al. Observation of the dynamical casimir effect in a superconducting circuit. *Nature* **479**, 376–379 (2011).
19. Yacomotti, A. M. et al. Nonadiabatic dynamics of the electromagnetic field and charge carriers in high-q photonic crystal resonators. *Phys. Rev. Lett.* **96**, 093901 (2006).
20. Preble, S. F., Xu, Q. & Lipson, M. Changing the colour of light in a silicon resonator. *Nat. Photonics* **1**, 293–296 (2007).
21. Upham, J., Tanaka, Y., Asano, T. & Noda, S. On-the-fly wavelength conversion of photons by dynamic control of photonic waveguides. *Appl. Phys. Express* **3**, 062001 (2010).
22. Kampfrath, T. et al. Ultrafast adiabatic manipulation of slow light in a photonic crystal. *Phys. Rev. A* **81**, 043837 (2010).
23. Castellanos Muñoz, M., Petrov, A. Y. & Eich, M. All-optical on-chip dynamic frequency conversion. *Appl. Phys. Lett.* **101**, 141119 (2012).
24. Kondo, K. & Baba, T. Dynamic wavelength conversion in copropagating slow-light pulses. *Phys. Rev. Lett.* **112**, 223904 (2014).
25. Dekker, R. et al. Ultrafast kerr-induced all-optical wavelength conversion in silicon waveguides using 1.55 μm femtosecond pulses. *Opt. Express* **14**, 8336–8346 (2006).
26. Agrawal, G. P., Baldeck, P. & Alfano, R. Temporal and spectral effects of cross-phase modulation on copropagating ultrashort pulses in optical fibers. *Phys. Rev. A* **40**, 5063–5072 (1989).
27. Li, J., Olsson, B.-E., Karlsson, M. & Andrekson, P. A. Otdm add-drop multiplexer based on xpm-induced wavelength shifting in highly nonlinear fiber. *J. Lightwave Technol.* **23**, 2654–2661 (2005).
28. Mehta, P., Healy, N., Day, T., Badding, J. V. & Peacock, A. Ultrafast wavelength conversion via cross-phase modulation in hydrogenated amorphous silicon optical fibers. *Opt. Express* **20**, 26110–26116 (2012).
29. Bloembergen, N. Laser-induced electric breakdown in solids. *IEEE J. Quant. Electron.* **10**, 375–386 (1974).
30. Yablonovitch, E. Self-phase modulation of light in a laser-breakdown plasma. *Phys. Rev. Lett.* **32**, 1101–1104 (1974).
31. Wood, W. M., Siders, C. & Downer, M. Measurement of femtosecond ionization dynamics of atmospheric density gases by spectral blueshifting. *Phys. Rev. Lett.* **67**, 3523–3526 (1991).
32. Lopes, N. et al. Laser pulse frequency up-shifts by relativistic ionization fronts. *Europhys. Lett.* **66**, 371–377 (2004).
33. Fan, L. et al. Integrated optomechanical single-photon frequency shifter. *Nat. Photonics* **10**, 766–770 (2016).
34. Del'Haye, P. et al. Optical frequency comb generation from a monolithic microresonator. *Nature* **450**, 1214–1217 (2007).
35. Li, Q., Davanço, M. & Srinivasan, K. Efficient and low-noise single-photon-level frequency conversion interfaces using silicon nanophotonics. *Nat. Photonics* **10**, 406–414 (2016).
36. Gaafar, M. A. et al. Reflection from a free carrier front via an intraband indirect photonic transition. *Nat. Commun.* **9**, 1447 (2018).
37. Beggs, D. M., Krauss, T. F., Kuipers, L. & Kampfrath, T. Ultrafast tilting of the dispersion of a photonic crystal and adiabatic spectral compression of light pulses. *Phys. Rev. Lett.* **108**, 033902 (2012).
38. Lee, K. et al. Linear frequency conversion via sudden merging of meta-atoms in time-variant metasurfaces. *Nat. Photonics* **12**, 765–773 (2018).
39. Shcherbakov, M. R. et al. Photon acceleration and tunable broadband harmonics generation in nonlinear time-dependent metasurfaces. *Nat. Commun.* **10**, 1345 (2019).
40. Gaburro, Z. Photonic energy lifters and event horizons with time-dependent dielectric structures. *J. Nanophotonics* **2**, 021853 (2008).
41. Silveirinha, M. & Engheta, N. Tunneling of electromagnetic energy through subwavelength channels and bends using ε-near-zero materials. *Phys. Rev. Lett.* **97**, 157403 (2006).
42. Engheta, N. Pursuing near-zero response. *Science* **340**, 286–287 (2013).
43. Liberal, I. & Engheta, N. Near-zero refractive index photonics. *Nat. Photonics* **11**, 149–158 (2017).
44. Alam, M. Z., De Leon, I. & Boyd, R. W. Large optical nonlinearity of indium tin oxide in its epsilon-near-zero region. *Science* **352**, 795–797 (2016).
45. Kinsey, N. et al. Epsilon-near-zero al-doped zno for ultrafast switching at telecom wavelengths. *Optica* **2**, 616–622 (2015).
46. Ferrera, M. & Carnemolla, E. G. Ultra-fast transient plasmonics using transparent conductive oxides. *J. Optics* **20**, 024007 (2018).
47. Capretti, A., Wang, Y., Engheta, N. & Dal Negro, L. Enhanced third-harmonic generation in si-compatible epsilon-near-zero indium tin oxide nanolayers. *Opt. Lett.* **40**, 1500–1503 (2015).
48. Agrawal, G. P. Nonlinear fiber optics. in *Nonlinear Science at the Dawn of the 21st Century. Lecture Notes in Physics*, Vol. 542 (Springer, 2000).
49. Gui, Y. et al. Towards integrated metatronics: a holistic approach on precise optical and electrical properties of indium tin oxide. *Sci. Rep.* **9**, 1–10 (2019).
50. Yang, Y. et al. Femtosecond optical polarization switching using a cadmium oxide-based perfect absorber. *Nat. Photonics* **11**, 390–395 (2017).
51. Saglamyurek, E. et al. Quantum storage of entangled telecom-wavelength photons in an erbium-doped optical fibre. *Nat. Photonics* **9**, 83–87 (2015).
52. Yanik, M. F. & Fan, S. Stopping light all optically. *Phys. Rev. Lett.* **92**, 083901 (2004).
53. Yoo, S. B. Wavelength conversion technologies for wdm network applications. *J. Lightwave Technol.* **14**, 955–966 (1996).
54. Caloz, C. et al. Electromagnetic nonreciprocity. *Phys. Rev. Appl.* **10**, 047001 (2018).
55. Sounas, D. L., Caloz, C. & Alu, A. Giant non-reciprocity at the subwavelength scale using angular momentum-biased metamaterials. *Nat. Commun.* **4**, 2407 (2013).
56. Giergiel, K., Dauphin, A., Lewenstein, M., Zakrzewski, J. & Sacha, K. Topological time crystals. *N. J. Phys.* **21**, 052003 (2019).
57. Bruno, V. et al. Broad frequency shift of parametric processes in epsilon-near-zero time-varying media. *Appl. Sci.* **10**, 1318 (2020).

Acknowledgements

R.W.B. C.L., Y.Z. and A.E.W. acknowledge support from DARPA (grant No. W911NF-18-0369). O.R. acknowledges the support of the Banting Postdoctoral Fellowship from the Natural Science and Engineering Research Council, Canada. This work was supported by the US Office of Naval Research and the Natural Science and Engineering Research Council, Canada. Note: while our paper was in review, a complementary paper was submitted and published[57]. In contrast to our work, they demonstrate wavelength conversion using four-wave mixing process in a time-varying ENZ thin film.

Author contributions

M.Z.A., J.U., and R.W.B. conceived the work after serendipitous observation of the effect in the laboratory by M.Z.A. M.Z.A. performed the first set of laboratory tests. M.Z.A., Y.Z., O.R., and J.U. designed the experiment. Y.Z. with help from M.Z.A., M.K., O.R., J.U., and C.L. performed laboratory measurements. Y.Z. with help from M.Z.A. performed data analysis and developed the numerical model. Y.Z and M.Z.A. wrote the first draft. All authors contributed to the discussion of the results and the preparation of the final version of the manuscript. A.E.W. and R.W.B. supervised the work.

Competing interests

The authors declare no competing interests.

Additional information

Supplementary information is available for this paper at https://doi.org/10.1038/s41467-020-15682-2.

Correspondence and requests for materials should be addressed to Y.Z.

Peer review information *Nature Communications* thanks the anonymous reviewers for their contribution to the peer review of this work. Peer reviewer reports are available.

Reprints and permission information is available at http://www.nature.com/reprints

Publisher's note Springer Nature remains neutral with regard to jurisdictional claims in published maps and institutional affiliations.

Supplementary Information

Broadband frequency translation through time refraction in an epsilon-near-zero material

Zhou *et al*.

Supplementary Information

Yiyu Zhou[1,†,*], M. Zahirul Alam[2,†], Mohammad Karimi[2], Jeremy Upham[2], Orad Reshef[2], Cong Liu[3], Alan E. Willner[3] and Robert W. Boyd[1,2]

[1]The Institute of Optics, University of Rochester, Rochester, New York 14627, USA

[2]Department of Physics, University of Ottawa, Ottawa, Ontario K1N 6N5, Canada

[3]Department of Electrical Engineering, University of Southern California, Los Angeles, California, 90089, USA

[†]These authors contributed equally

[*]corresponding author: yzhou62@ur.rochester.edu

Supplementary Note 1: Experimental setup

We use a wavelength-tunable optical parametric amplifier (TOPAS prime, Spectra Physics) pumped by an amplified Ti:sapphire laser (Mai Tai, Spectra Physics) as the ultrafast pulse source. A 45:55 pellicle beamsplitter (BP245B3, Thorlabs) is used to split the input beam, and a high-precision translation stage (DDSM100, Thorlabs) is used to tune the delay time between pump and probe pulses. We use a thin film polarizer mounted on a rotation stage and a Glan-Taylor polarizing beam splitter to control the pulse intensity while keeping the polarization to be *p*-polarized. We use a multimode fiber with 50 μm core diameter to collect the probe pulse after the sample and use an optical spectrum analyzer to record the spectra of the probe.

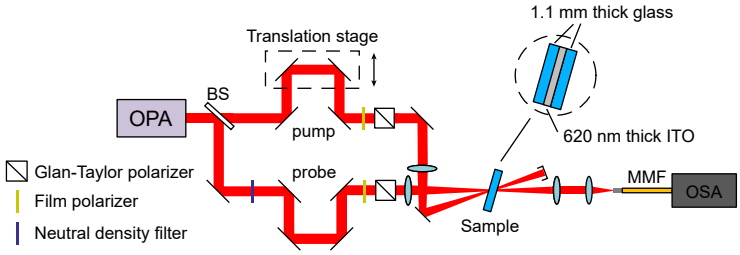

Supplementary Figure 1. The schematic of the experimental setup. In the pump beam arm, we rotate the first polarizer to control the peak pump intensity. BS, pellicle beamsplitter. OPA, optical parametric amplifier. OSA, optical spectrum analyzer. MMF, multimode fiber.

Supplementary Note 2: Numerical simulation

We use a split-step Fourier method to solve the nonlinear Schrödinger equation (NLSE)[1] to model the nonlinear interactions between the pump and the probe beam pulses propagating through the ITO sample. We ignore all nonlinear optical effects higher than the third-order effects[2]. The propagation of the probe pulse through the time-varying ITO can be described as[3]

$$\frac{\partial A}{\partial z}+\beta_1\frac{\partial A}{\partial t}+\mathrm{i}\frac{\beta_2}{2}\frac{\partial^2 A}{\partial t^2}=\mathrm{i}\frac{\omega_0}{c}\Delta n_{\mathrm{eff}}(t-t_{\mathrm{d}},I_{\mathrm{pump}}(t))A, \tag{1}$$

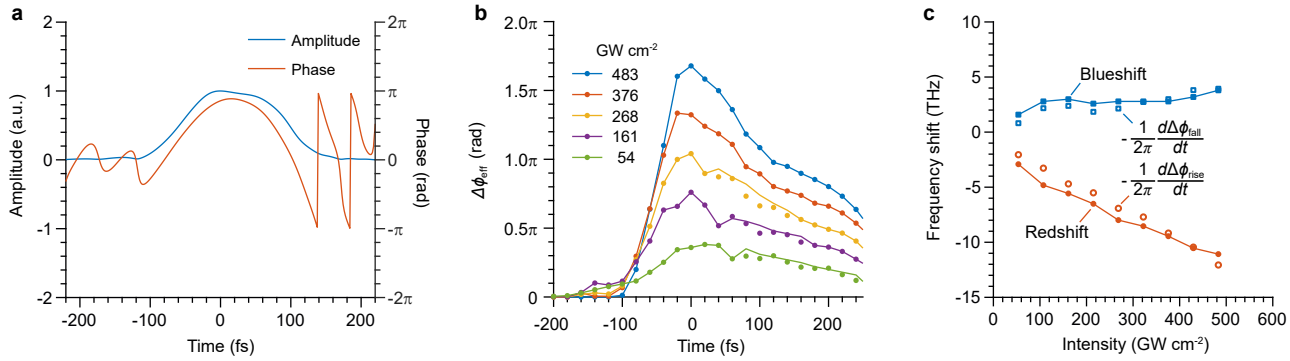

Supplementary Figure 2. **a**, Amplitude and phase of the optical pulses at 1235 nm retrieved by frequency-resolved optical gating. **b**, Numerically retrieved nonlinear phase variations $\Delta\phi_{\mathrm{eff}}(t)$ at different pump intensities. The dots represent the numerical results and the solid lines connecting the dots are to facilitate visualization. **c**, The experimentally measured redshifts and blueshifts as a function of pump intensity are represented by the solid lines, and the calculated maximum local frequency shifts are represented by hollow circles.

where $A(z,t)$ is the slowly varying envelope of the probe pulse, $\beta_1 \equiv (1/v_{\mathrm{g}})$ is the inverse of the group velocity, $\beta_2 \equiv \frac{\partial}{\partial\omega}(1/v_{\mathrm{g}})$ is the group velocity dispersion, c is the speed of light in vacuum, t_{d} is the pump-probe delay time, and ω_0 is the angular frequency of the light beams. The effective time-dependent refractive index index $\Delta n_{\mathrm{eff}}(t, I_{\mathrm{pump}})$ on the right-hand side is a function of pump intensity and the delay time between the pump and the probe. This term acts as the driving term for the nonlinear pulse propagation and is responsible for the frequency translation. The relative permittivity of ITO around its epsilon-near-zero spectral range can be modeled by a Drude function as[4]

$$\varepsilon(\omega) = \varepsilon_\infty - \omega_{\mathrm{p}}^2/(\omega^2 + \mathrm{i}\gamma\omega), \tag{2}$$

where $\varepsilon_\infty = 3.80$, $\omega = 2\pi c/\lambda$ is the frequency of light, $\omega_{\mathrm{p}} = 2\pi\cdot 473$ THz is the plasma frequency, and $\gamma = 0.0468\cdot 2\pi\cdot 473$ THz is the damping rate. The refractive index of ITO can thus be expressed as $n(\omega) = \sqrt{\varepsilon(\omega)}$. The dispersion coefficients can be calculated as $\beta_m = \left(\frac{d^m\beta}{d\omega^m}\right)_{\omega=\omega_0}$, where $\beta(\omega) = \mathrm{Re}(n(\omega))\omega/c$. At $\lambda = 1235$ nm we have $\beta_1 = 1.53\times 10^7$ fs m^{-1} and $\beta_2 = 1.10\times 10^8$ fs^2 m^{-1}. The dispersion length is found to be $L_{\mathrm{D}} = T_0^2/\beta_2 = 47.1$ μm, where $2\sqrt{\ln(2)}T_0 = 120$ fs is the FWHM pulse width. Since the dispersion length is two orders of magnitude larger than the ITO thickness of 0.62 μm, we neglect higher-order dispersion terms.

For the numerical simulation we ignore the changes in $\Delta n_{\mathrm{eff}}(t)$ that occur at the time scale of the oscillation of the carrier waves of the pump pulse. We only take into account the pump-envelope-dependent changes in the refractive index. Thus, in our simulation we approximate $\Delta n_{\mathrm{eff}}(t)$ as a function of the envelope of the pump pulse only. We use an iterative least squares curve fitting algorithm to extract an approximate shape of pump-intensity-dependent $\Delta n_{\mathrm{eff}}(t)$ that results in the experimentally obtained output probe spectra for a fixed pump intensity as follows: (1) We begin with an initial guess $\Delta n_{\mathrm{eff}}^1(t)$. For j-th iteration, the corresponding index change is denoted as $\Delta n_{\mathrm{eff}}^j(t)$. (2) For the index change $\Delta n_{\mathrm{eff}}^j(t)$ and a specific pump-probe delay time t_{d}', we use $\Delta n_{\mathrm{eff}}^j(t - t_{\mathrm{d}}')$ in Supplementary Eq. (1) and perform the split-step Fourier method to generate an output pulse $A^j(z_1, t; t_{\mathrm{d}}')$,

where $z_1 = 620$ nm. The output spectrum can be calculated via Fourier transform as $S^j(f,t_d') = |\int A^j(z_1,t;t_d')\exp(-i2\pi ft)\,dt|^2$. We repeat this procedure for different delay times and therefore obtain the two-dimensional spectrogram $S^j(f,t_d)$ with -200 fs $\leq t_d \leq 200$ fs. (3) We use a fitting algorithm (lsqcurvefit, MATLAB) to fit $S^j(f,t_d)$ to the experimental data $S^{exp}(f,t_d)$ by adjusting $\Delta n_{eff}^j(t)$. In other words, $\Delta n_{eff}^j(t)$ is the parameter to be tuned iteratively. The final results of $S^j(f,t_d)$ at different pump intensities are presented in Fig. 3(d-f) in the manuscript.

In order to obtain the temporal amplitude and phase of the input probe pulses at the wavelengths of interest, i.e. $A(z=0,t)$, we performed a series of frequency-resolved optical gating (FROG) measurements[5]. In our simulation we always assume a homogeneous index change throughout the entire ITO film for simplification. We also ignore the time difference of the index change between the front and the back ends of the sample since the transit time through the sample is roughly two-orders of magnitude smaller than the temporal width of the pump pulse. We also ignore the Fresnel-reflection- and absorption-induced change in the pump intensity inside the sample for simplification. In addition, we also ignore nonlinear change in dispersion. The experimentally measured temporal amplitude and phase of the input probe pulse at 1235 nm is shown in Supplementary Fig. 2a.

An alternative way to understand the effect of index change is to use the concept of a local frequency shift. The local frequency shift can be used as an approximate estimation of spectral shift and can be expressed as[6]

$$\Delta f(t) = \frac{1}{2\pi}\Delta\omega(t) = -\frac{1}{2\pi}\frac{d\Delta\phi_{eff}(t)}{dt}, \tag{3}$$

where the nonlinear phase variation induced by Δn_{eff} is $\Delta\phi_{eff}(t) = k\cdot L\cdot\Delta n_{eff}(t)$, where $k = 2\pi/\lambda$ is the wavenumber, and $L = 620$ nm is the ITO thickness. The retrieved phase variation $\Delta\phi_{eff}$ is displayed for different peak pump intensities in Supplementary Fig. 2b. For a given $\Delta\phi_{eff}$, the maximum local frequency redshift is determined by the rising edge of the nonlinear phase change as $\Delta f_{red} = \min(\Delta f(t)) = -\frac{1}{2\pi}\frac{d\Delta\phi_{rise}}{dt}$, while the maximum local frequency blueshift is determined by the falling edge as $\Delta f_{blue} = \max(\Delta f(t)) = -\frac{1}{2\pi}\frac{d\Delta\phi_{fall}}{dt}$. The numerically retrieved maximum local frequency shifts at different pump intensities are shown in Supplementary Fig. 2c. The retrieved maximum local frequency shifts are in good agreement with the experimentally measured frequency shifts.

Supplementary Note 3: Additional time refraction effects and unnormalized spectra

Since the focus of this work is on frequency translation, we presented spectral data with normalized amplitude in the main text. However, time refraction also affects the amplitude of the frequency-translated pulse[7]. Let us consider the simplest time-refraction model — a Gaussian pulse with carrier frequency ω_0 and pulse width T_0 is travelling through a medium whose

refractive index changes from n_1 to n_2. We assume that the longitudinal length of the medium is larger than the longitudinal length of the pulse. In such an idealized case the input (E_{in}) and output (E_{out}) pulses can be expressed as[8]

$$E_{\text{in}} = E_0 \exp(-\frac{t^2}{2T_0^2}) \exp(-\text{i}\omega_0 t), \qquad E_{\text{out}} = (\frac{n_1}{n_2} E_0)\ \exp(-\frac{t^2}{2(T_0 n_2/n_1)^2})\ \exp(-\text{i}\frac{n_1}{n_2}\omega_0 t). \tag{4}$$

The above simple model shows that the time refraction effect can modify amplitude, temporal width (by Fourier relation the spectral width), and the central frequency. Therefore, the relative changes in spectral amplitude may also be of interest. Below we present the spectral data for five different probe wavelengths for various pump-probe delays in Supplementary Fig. 3-7, where the spectral peak magnitude in the absence of pump pulse is normalized to unity. However, it should be noted that in addition to time refraction there are several other competing effects in ITO that can significantly modulate the transmittance of the probe pulse. Since the ITO has a small linear index and exhibits a large nonlinear index change, the Fresnel reflection coefficients exhibit strong time-dependent variations. In addition, due to saturable absorption, the imaginary part of the refractive index and, consequently, the loss in ITO can drop significantly in the presence of a pump pulse. Thus the spectral amplitude of the probe for a given pump-probe delay and pump intensity depends on time-refraction effects, nonlinear changes in Fresnel reflection coefficient, and changes in absorption. Therefore a sophisticated model is required to isolate these three effects to accurately quantify the effect of time refraction on the amplitude, which is beyond the scope of this work. Nevertheless, it can be noticed that for all wavelengths of interest, the transmittance of the probe beam significantly increases when the probe is blueshifted.

We also note that the absorption loss in ITO in the ENZ spectral range is large compared to standard dielectric materials. We note that a fair figure of merit for such a medium should be the magnitude of nonlinear change over one absorption length. Clearly ITO cannot be used to make optical fibre or nanophotonics waveguides of hundreds of microns in length. The crucial advantage of these ENZ materials over other conventional materials is that one needs to propagate over only a sub-micron distance in a nonlinear ENZ material for a comparable effect that is achieved by a hundreds of microns long nanophotonic waveguide made of a conventional photonics material. It should be noted that for this work we are using a commercially available sample that has never been optimized for the purpose of this work. In addition, there are still many opportunities to further enhance the performance of ENZ materials. A few promising routes are: i) use an ENZ material with higher electron mobility, ii) nanostructure the ENZ material or include plasmonic systems to achieve higher effective index change within reduced thickness and loss, iii) integrate ENZ material with optical waveguides as the cladding, etc. We also note that in the presence of strong pump the transmittance of the probe can actually increase due to the increased refractive index and reduced loss. Finally, we note that the use of optical amplifiers to boost a weak signal is a standard system protocol. Furthermore, the recent advancement in short pulse amplification might also be of interest for particular applications[9].

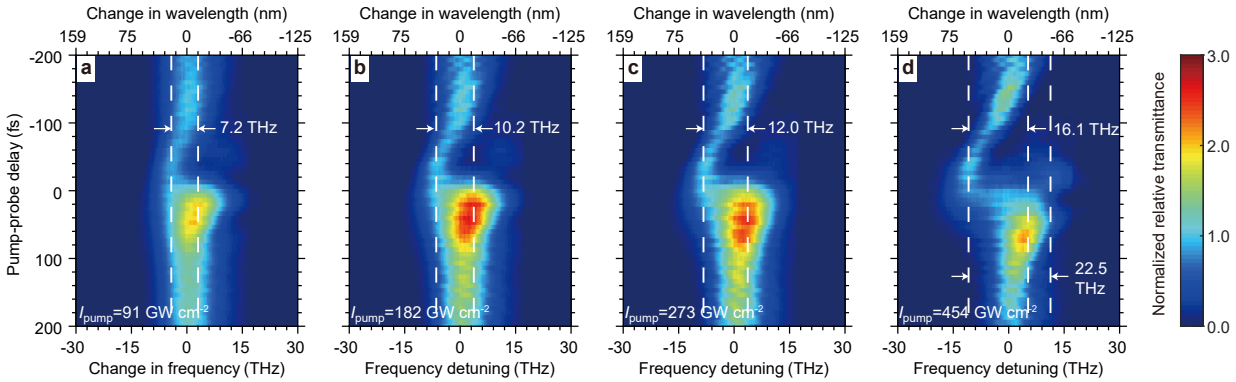

Supplementary Figure 3. **a-d**, The experimentally measured spectra of 1184 nm probe pulse at different pump intensities. The spectral peak of the probe beam in the absence of pump beam is normalized to unity.

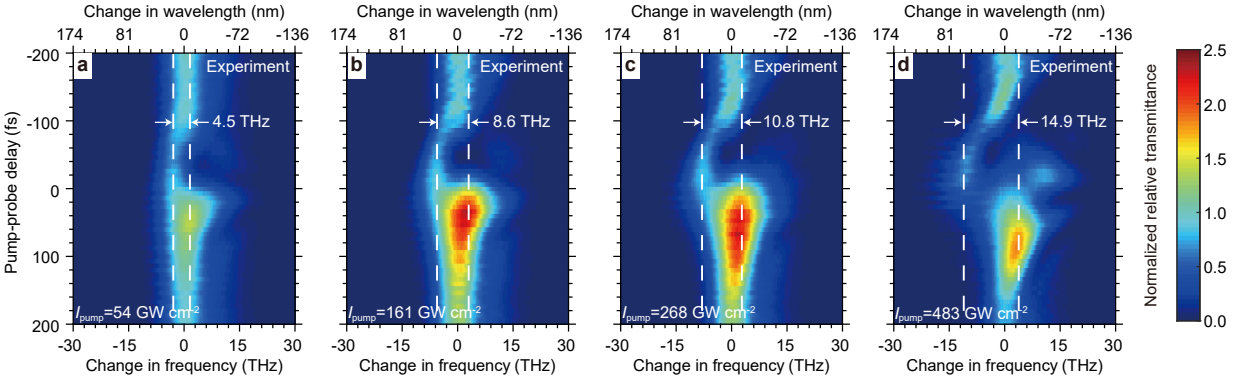

Supplementary Figure 4. **a-d**, The experimentally measured spectra of 1235 nm probe pulse at different pump intensities. The spectral peak of the probe beam in the absence of pump beam is normalized to unity.

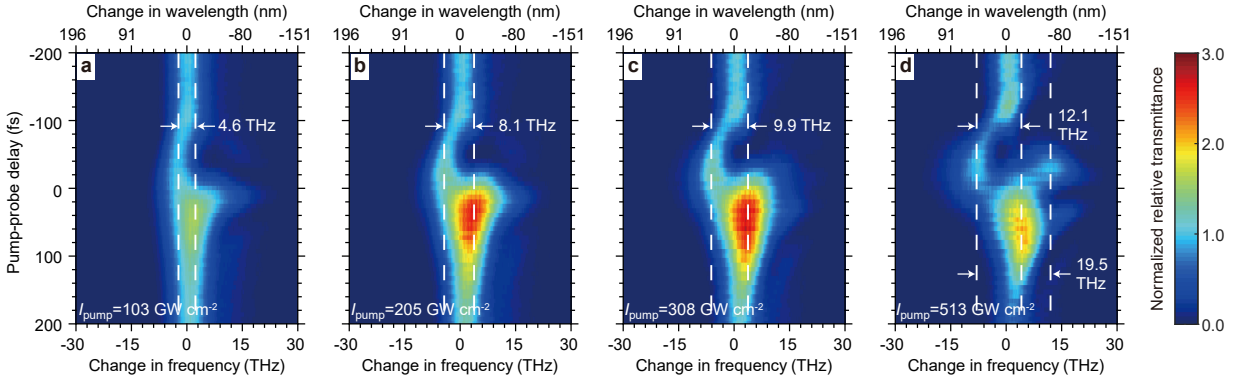

Supplementary Figure 5. **a-d**, The experimentally measured spectra of 1305 nm probe pulse at different pump intensities. The spectral peak of the probe beam in the absence of pump beam is normalized to unity.

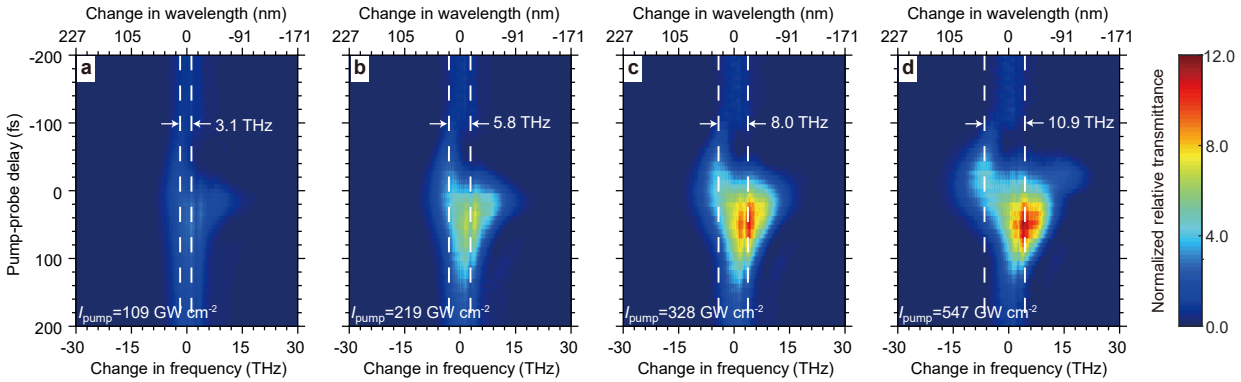

Supplementary Figure 6. **a-d**, The experimentally measured spectra of 1398 nm probe pulse at different pump intensities. The spectral peak of the probe beam in the absence of pump beam is normalized to unity.

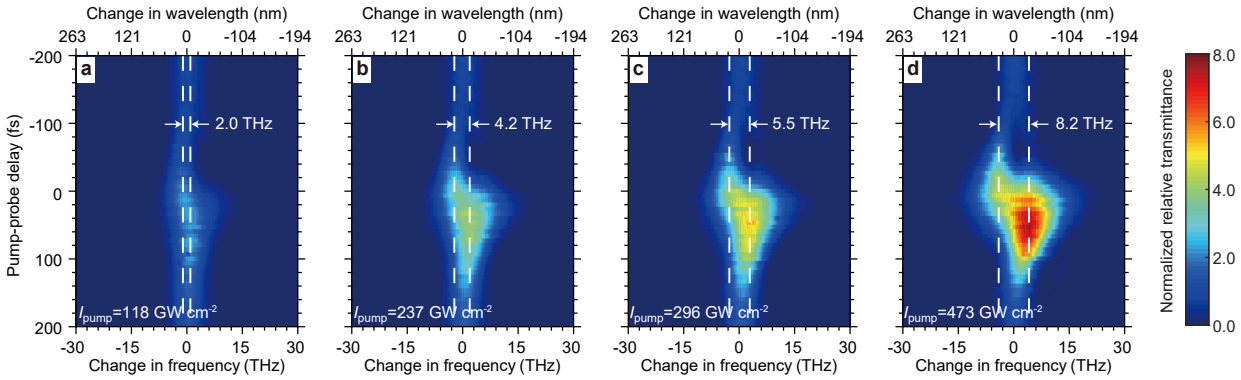

Supplementary Figure 7. **a-d**, The experimentally measured spectra of 1495 nm probe pulse at different pump intensities. The spectral peak of the probe beam in the absence of pump beam is normalized to unity.

Supplementary Note 4: Effects of fifth-order nonlinearity

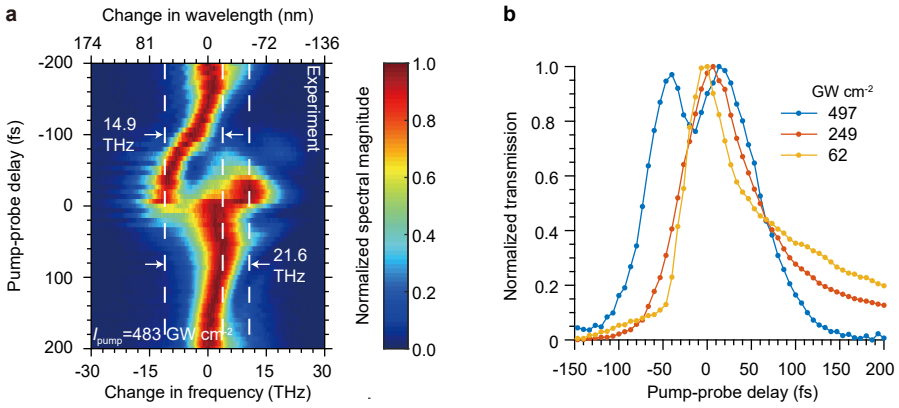

Supplementary Figure 8. **a**, The experimentally measured probe spectrogram at the peak pump intensity of 483 GW cm^{-2}. **b**, The experimentally measured probe transmission at different pump intensities as a function of pump-probe delay time.

At a high pump intensity of greater than 450 GW cm^{-2} close to the zero permittivity wavelength we observe onsets of higher-order nonlinear optical effects. For example, at $\lambda_0 = 1235$ nm at a pump intensity of 480 GW cm^{-2} we observe a relatively large blueshifted peak as shown in Supplementary Fig. 8a due to an effective fifth-order nonlinear optical process. In a pump-probe transmission measurement this effective fifth-order process leads to a sudden drop in the transmission of the probe Supplementary Fig. 8b. From these results we conclude that the effective fifth-order process has an opposite sign to that of the effective third-order process and that the relevant time scales for the fifth-order-nonlinearity-induced blue shift is much shorter compared to the effective third-order-nonlinearity-induced blue shift at lower intensities.

Supplementary Note 5: Normalized spectra at other wavelengths

Here, we provide the detailed measurement results for pump-probe wavelengths ranging from $\lambda = 1000$ nm to 1500 nm in Supplementary Fig. 9-14.

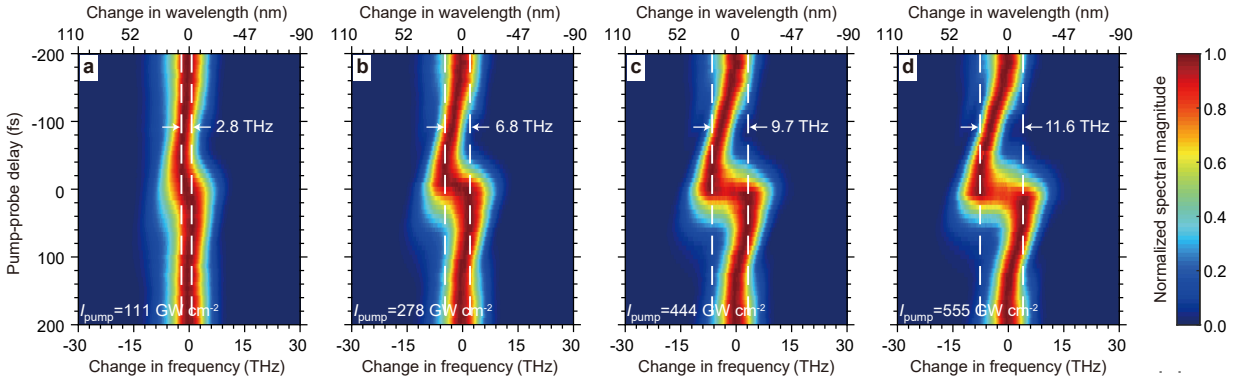

Supplementary Figure 9. a-d, The experimentally measured spectra of 1000 nm probe pulse at different pump intensities. The magnitudes of the measured maximum redshift and blueshift are denoted by the corresponding white dashed lines.

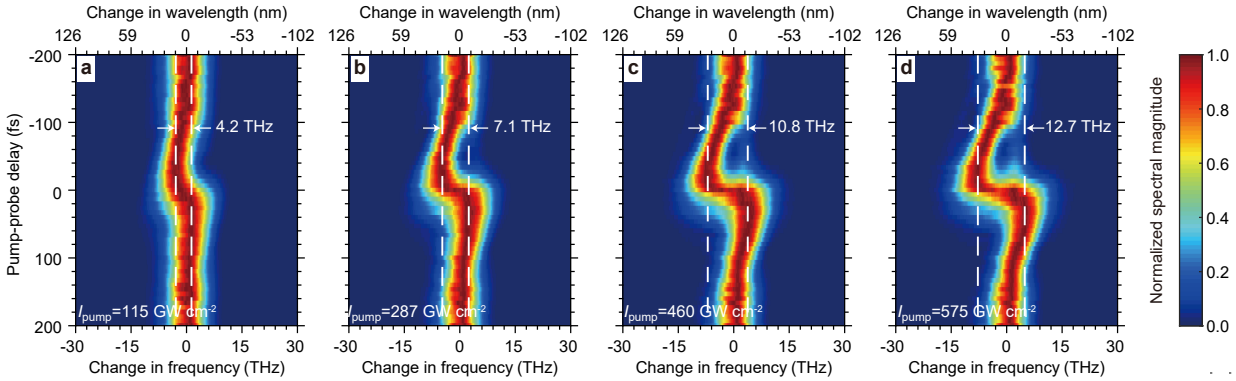

Supplementary Figure 10. a-d, The experimentally measured spectra of 1060 nm probe pulse at different pump intensities. The magnitudes of the measured maximum redshift and blueshift are denoted by the corresponding white dashed lines.

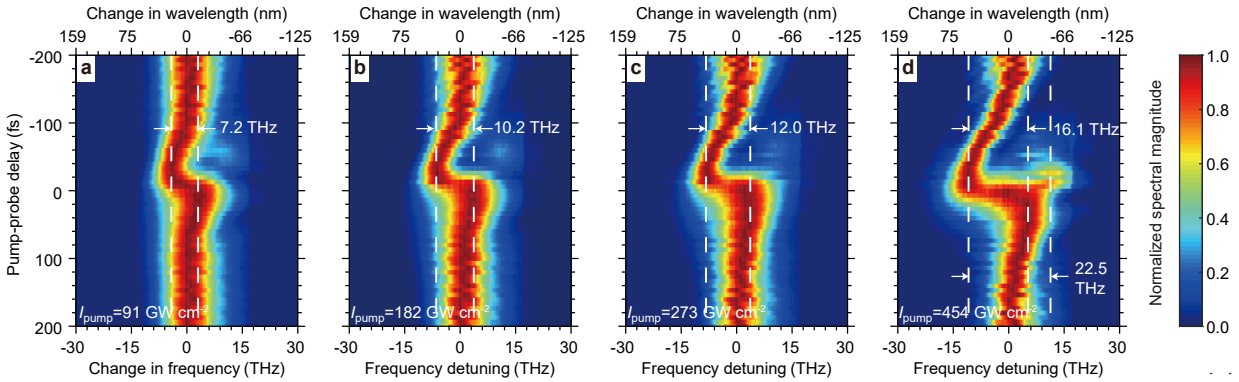

Supplementary Figure 11. a-d, The experimentally measured spectra of 1184 nm probe pulse at different pump intensities. The magnitudes of the measured maximum redshift and blueshift are denoted by the corresponding white dashed lines. The subpanel **d** also shows the an additional blueshifted peak (6.4 THz) due to the effective fifth-order nonlinear process.

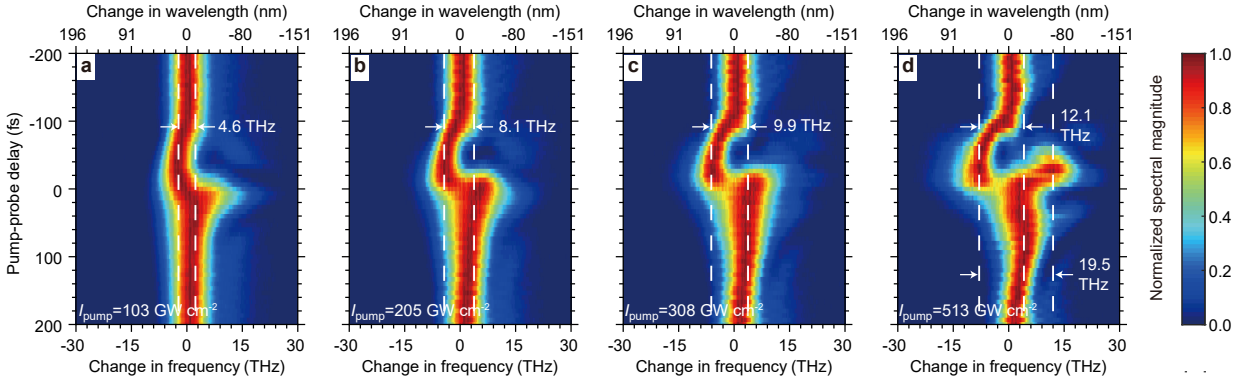

Supplementary Figure 12. a-d, The experimentally measured spectra of 1305 nm probe pulse at different pump intensities. The magnitudes of the measured maximum redshift and blueshift are denoted by the corresponding white dashed lines.The subpanel **d** also shows the an additional blueshifted peak (7.4 THz) due to the effective fifth-order nonlinear process.

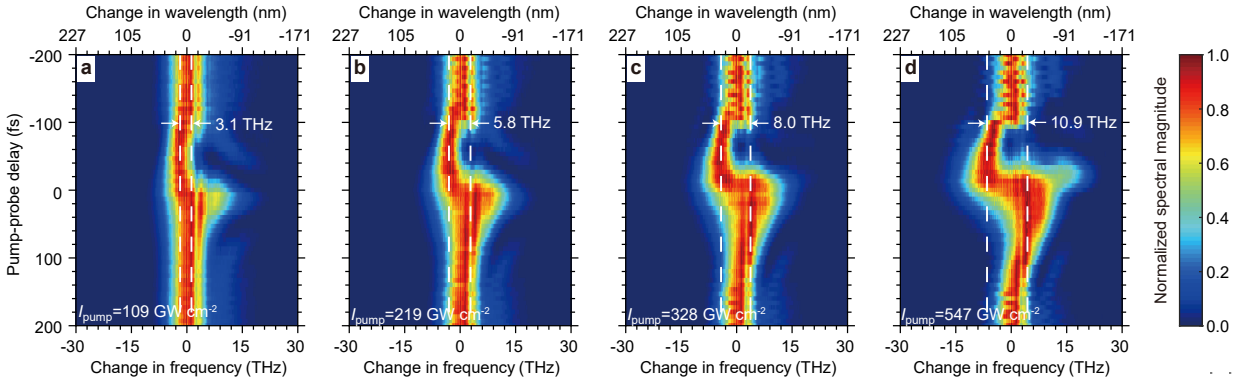

Supplementary Figure 13. a-d, The experimentally measured spectra of 1398 nm probe pulse at different pump intensities. The magnitudes of the measured maximum redshift and blueshift are denoted by the corresponding white dashed lines.

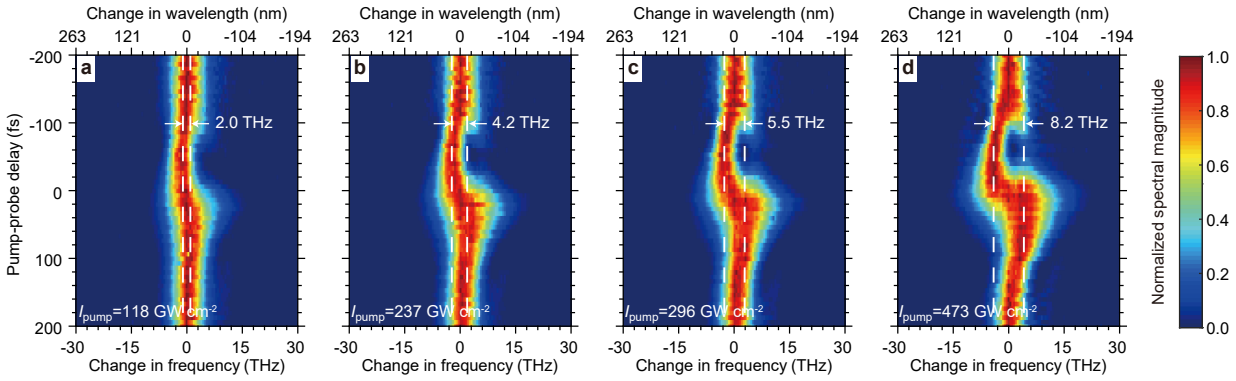

Supplementary Figure 14. a-d, The experimentally measured spectra of 1495 nm probe pulse at different pump intensities. The magnitudes of the measured maximum redshift and blueshift are denoted by the corresponding white dashed lines.

Supplementary Note 6: Analysis of the air gap between ITO films

In our experiment, we form a 620-nm-thick medium by sandwiching two commercially available 310-nm-thick ITO films deposited on 1.1-mm-thick glass. However, a white-light interferometric measurement reveals that there remains an air gap between two layers of the ITO thin films. We measure the air gap to be roughly 2200 nm thick. Air has a higher refractive index than ITO at the wavelengths of interest (e.g. $n_{\mathrm{ITO}} = 0.42 + 0.42\mathrm{i}$ at $\lambda_0 = 1240$ nm) and the air gap has a thickness slightly larger than the free-space wavelength. Thus one may expect that there is an unintended weak cavity effect due to thin film interference effects for our structure. However we posit that this unintended air gap affects our results minimally for two reasons. First, compared to ITO the nonlinear response of the air gap at the pump intensities relevant for this experiment is negligible. Second, the effective third-order nonlinear response of ITO leads to an increase in refractive index at all wavelengths of interest in this work. Thus at high pump intensities for which the frequency translation of the probe pulses are the largest, the thin-film interference effects effectively disappears.

Supplementary References

1. Agrawal, G. P. *Nonlinear fiber optics* (Springer, 2000).

2. Boyd, R. W. *Nonlinear optics* (Elsevier, 2003).

3. Plansinis, B. W., Donaldson, W. R. & Agrawal, G. P. What is the temporal analog of reflection and refraction of optical beams? *Phys. Rev. Lett.* **115**, 183901 (2015).

4. Alam, M. Z., De Leon, I. & Boyd, R. W. Large optical nonlinearity of indium tin oxide in its epsilon-near-zero region. *Science* **352**, 795–797 (2016).

5. Trebino, R. et al. Measuring ultrashort laser pulses in the time-frequency domain using frequency-resolved optical gating. *Rev. Sci. Instrum.* **68**, 3277–3295 (1997).

6. Dekker, R. et al. Ultrafast kerr-induced all-optical wavelength conversion in silicon waveguides using 1.55 μm femtosecond pulses. *Opt. Express* **14**, 8336–8346 (2006).

7. Xiao, Y., Maywar, D. N. & Agrawal, G. P. Reflection and transmission of electromagnetic waves at a temporal boundary. *Opt. Lett.* **39**, 574–577 (2014).

8. Xiao, Y. *Propagation of optical pulses in dynamic media: a time transformation method* (PhD thesis, University of Rochester, 2014).

9. Vampa, G. et al. Light amplification by seeded kerr instability. *Science* **359**, 673–675 (2018).